IEEE Open Journal of
Power Electronics

Received 29 March 2024; revised 6 May 2024; accepted 24 May 2024. Date of publication 3 June 2024;
date of current version 12 June 2024. The review of this article was arranged by Associate Editor Rafael Pena-Alzola.

Digital Object Identifier 10.1109/OJPEL.2024.3408272

A Partially Rated LC Trap Type AC Filter for Grid-Tied Voltage Source Converters

SRINIVAS GULUR [1] (Member, IEEE), VISHNU MAHADEVA IYER [2] (Senior Member, IEEE), AND SUBHASHISH BHATTACHARYA [3] (Fellow, IEEE)

[1]Archer Aviation, San Jose, CA 95134 USA
[2]Department of Electrical Engineering, Indian Institute of Science, Bangalore 560012, India
[3]Department of Electrical and Computer Engineering, NC State University, RaleighNC 27695 USA

CORRESPONDING AUTHOR: SRINIVAS GULUR (e-mail: sgulurncsu@gmail.com).

ABSTRACT *AC* power filters play an important role in limiting the high-frequency current harmonics injected by grid-tied voltage source converters (VSCs). Amongst the various types of filters, *LCL* filters with integrated *LC* traps have become popular due to their ability to achieve a size reduction of the grid side inductor while demonstrating a similar current harmonic mitigation performance as a traditional *LCL* filter. In this article, a passively damped filter network with a partially rated *LC* trap (also referred to as the *L-PT-L* filter) is proposed and delineated. The proposed *L-PT-L* filter provides a −60 dB/dec roll-off characteristics at frequencies greater than switching frequency. Additionally, it is also demonstrated that this proposed *L-PT-L* filter has smaller voltage ratings for two of its shunt-connected capacitor components due to the specific placement of the damping resistor. A systematic analysis of the proposed *L-PT-L* filter is elucidated to design and select the component parameters. Steady-state and transient experimental results captured from a grid-tied 2-Level, 3ϕ VSC prototype are provided to validate the grid current harmonic filtering capability, reduced voltage ratings of the two shunt capacitors and passive damping performance of the proposed *L-PT-L* filter. The proposed approach can achieve 19% and 36% filter shunt branch volume reduction for low voltage (208 V, 60 Hz) and medium voltage (4.16 kV, 60 Hz) grid-tied inverter systems, respectively, compared to state-of-the-art *LCL* filters with integrated *LC* traps.

INDEX TERMS Differential mode (DM) filter, *LCL* filter, *L-C-TL* filter, *LC* trap filter, *LLCL* filter, *LT-C-L* filter, *L-T-L* filter, passive damping, power filter, voltage source inverter, voltage source rectifier.

I. INTRODUCTION

The last few years have seen a phenomenal rise in the usage of grid-tied voltage source converters (VSC) in a wide variety of applications [1]. The pulse width modulation (PWM) of such converters causes unwanted current harmonics at switching frequency, its harmonics, and side bands. These current harmonic components are mitigated by typically interfacing a differential mode (DM) or an *AC* power filter between the power converter and the utility grid to meet the recommended IEEE 519-2014 standard [2] on power quality, as illustrated in Fig. 1. Therefore, the selection of the power filter can have a significant impact on the size, cost, and losses of the grid-tied power conversion system.

Traditionally, an *AC* filter was implemented using an inductor (*L*) due to the simplicity achieved during the operation and control of the grid-tied VSC. This changed with the adoption of *LCL* filters, which have considerable benefits in terms of size and performance as compared to a simple *L* filter [3], [4]. To further reduce the size and cost of the grid side inductor used in *LCL* filters, integration of various types of *LC* trap networks within *LCL* filters have generated significant research interest in the last several of years [5], [6], [7], [8], [9], [10], [11], [12], [13]. The *L* and *C* in a trap filter can be connected in series or parallel based on the required circuit configuration. One of the most popular solutions is to replace the *C* of the *LCL* filter with a series *LC* trap filter. Ideally, this *LC* branch can be tuned to provide a zero impedance path to the dominant (switching) frequency current component. Such a filter is generally referred to as the *LLCL* filter, and a detailed design was presented in [5]. Alternatively, it is possible to

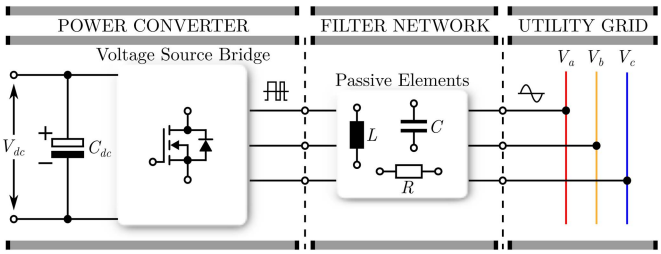

FIGURE 1. A 3ϕ voltage source converter (VSC) based power conversion system interfaced to the utility grid using a passive filter network.

achieve a similar performance as that of the *LLCL* filter with the usage of an *LCCL* filter [8], [9]. The *LCCL* is typically realized by using a parallel *LC* trap filter instead of the grid side inductor in a *LCL* filter. In this case, the parallel *LC* trap filter provides a very high impedance to the switching frequency current component of the grid current. Although both the *LLCL* and *LCCL* filters can suppress the switching frequency component in the grid current, it is worth noting that the higher frequency current components (switching frequency multiples and its side-bands) are attenuated by only −20 dB/dec roll-off rate when utilizing any one of these two filters. An undamped *LCL* filter, on the other hand, provides a −60 dB/dec attenuation to grid current harmonics across the frequency spectrum. This assumes significance when current harmonic multiples of switching frequency have to be attenuated to either meet IEEE 519-2014 / IEEE 1547-2018 harmonic distortion recommendations or electromagnetic interference (EMI) compliance limits dictated by FCC Part 15 or CISPR 11/32 [14].

An alternative approach is to add multiple *LC* trap branches by replacing the *C* in the *LCL* filter (referred to as the *L-T-L* filter, where *T* refers to *LC* traps) to further attenuate the multiples of the switching frequency harmonics in the grid side current while still only providing a −20 dB/dec high-frequency roll-off rate attenuation characteristics [15]. One of the limitations of such a scheme is that this filter may need to be redesigned to limit the fundamental frequency reactive current in the shunt branch due to several trap capacitors. Additionally, all the shunt trap capacitors need to be rated for the full per-phase fundamental grid voltage, which can impact the voltage rating of these components. It is possible to achieve a −60 dB/dec high-frequency roll-off performance with the *LCCL* by adding an additional inductor on the grid side (also called as the *L-C-TL* filter). A detailed analysis for the *L-C-TL* filter is provided in [8], [9]. Another interesting configuration is the *LT-C-L* filter where the parallel *LC* trap filter is inserted in series with the inverter side inductor (of the *LCL* filter) [6], [7]. Such a configuration can also provide a −60 dB/dec high-frequency attenuation to the unwanted grid current harmonic components. Although both the *L-C-TL* and *LT-C-L* filters offer very good current harmonic attenuation performance at high frequencies, the inductor used in the *LC* trap filter has to be rated for the fundamental current component. This can potentially impact the overall size of the *AC* filter, especially in high-power applications. Alternatively, it is possible to add an additional capacitor in parallel with *LC* trap of the *LLCL* filter to achieve a −60 dB/dec high-frequency attenuation characteristics [10], [16]. Such a *LCL-LC* filter is an attractive solution since the inductor size of the *LC* trap filter can be reduced as it needs to be rated to handle only the switching frequency current component. Unfortunately, the shunt capacitors in such a filter need to be rated to handle the full per-phase fundamental grid voltage component. This can become an important factor if multiple *LC* trap filters are incorporated within the shunt branch of such a filter [16].

Apart from achieving high-frequency attenuation characteristics for the *LC* trap-based *AC* filters, it is equally important to suppress the resonances caused by their impedance networks. It is well known that these resonances can be damped actively using feedback control techniques if they lie within the system control bandwidth or else passively by adding a physical resistive impedance [15], [17], [18], [19], [20]. Passive damping techniques increase the overall losses of the *AC* filter but are generally straightforward in their implementation. They do not require additional sensors or advanced feedback control-based solutions compared to active damping strategies. The passive damping schemes typically deal with the various placement strategies of the damping resistors within the *AC* filter. Integration of the damping resistors in the *AC* filters has to be analyzed carefully since it is generally important to preserve the high-frequency attenuation characteristics and limit the losses in the resistor while achieving the desired damping performance. Amongst the various passive damping methods, an *RC*-based damping scheme is fairly popular and is widely used with various types of *AC* filter configurations [6], [15], [21]. This is because such an *RC* damping network does not impact the high-frequency roll-off characteristic of the *AC* filters and can minimize the power loss in the damping resistor [6], [16]. This additional *RC* damping branch is connected in parallel with the shunt branch in all the different *LC* trap-based *AC* filters [15], [22]. With such an *RC* damping strategy, all the shunt capacitors in the *LC* trap-based filters must be rated to handle the fundamental frequency voltage component. In addition, the *RC* damping branch may increase the fundamental frequency reactive current component, necessitating a filter redesign. Further, passive damping can protect the inductive and capacitive components of the *AC* filters from sudden *AC* grid voltage transients when the grid-tied converter is switched off [19].

This work proposes, analyzes and elucidates a passively damped *AC* filter with a partially rated *LC* trap (named in this article as the *L-PT-L* filter) for grid-tied VSCs as shown in Fig. 2. The key advantages of the proposed *L-PT-L* filter are listed below:

1) This filter can provide a −60 dB/dec high-frequency roll-off attenuation characteristics to unwanted grid

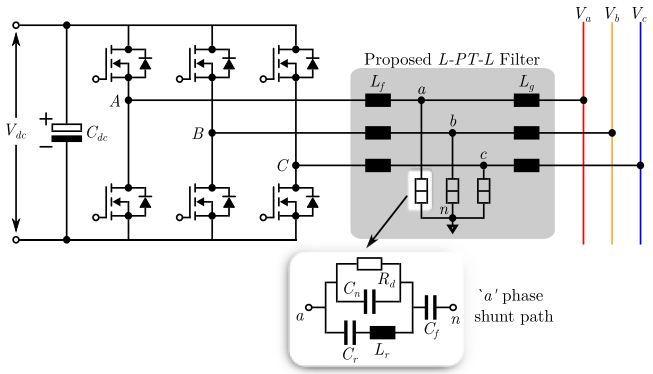

FIGURE 2. 3ϕ, 2-level grid-tied VSC with proposed *L-PT-L* filter network.

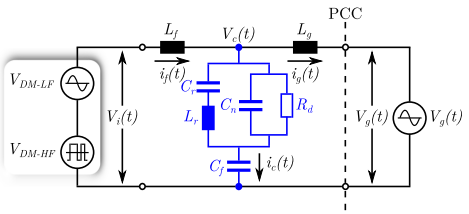

FIGURE 3. A per-phase equivalent circuit representation of the proposed *L-PT-L* filter network for a grid-tied VSC is depicted in this figure. PCC refers to point of common coupling.

current harmonic components at frequencies greater than the switching frequency.

2) Further, it is also demonstrated that the specific placement of the damping resistor aids in the reduction of the voltage ratings of two capacitors connected in the shunt path. This can have a significant impact on the size of the *AC* filter if several *LC* trap filters tuned at multiples of the switching frequency are employed to further mitigate the high-frequency harmonics in the grid current.
3) Though multiple capacitors are used in the proposed *AC* filter network, the fundamental frequency reactive current through the shunt path of the filter can be limited by appropriately selecting the main shunt capacitor component.

II. PROPOSED *L-PT-L* FILTER

The single-phase equivalent representation of the proposed *L-PT-L* filter for a grid-tied VSC is illustrated in Fig. 3. The per-phase switching voltage of the VSC, $V_i(t)$, consists of both fundamental frequency (V_{DM-LF}) as well as PWM frequency (V_{DM-HF}) components. The converter side, shunt, and grid side currents are represented by $i_f(t)$, $i_c(t)$, and $i_g(t)$ respectively. The admittance transfer function, $i_g(s)/V_i(s)$, for the proposed filter structure is given in (1) and describes the per-phase relationship between $V_i(s)$ and $i_g(s)$.The shunt path, converter side inductor, and grid side inductor impedances are denoted by $Z_s(s)$, $Z_f(s)$, and $Z_g(s)$,

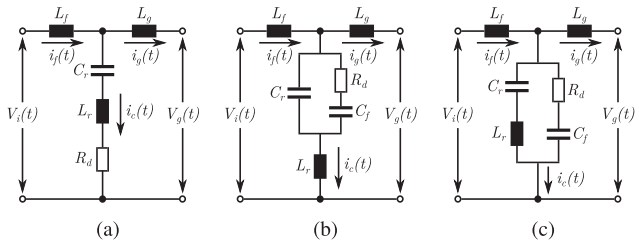

FIGURE 4. Popular shunt based passive damping schemes for the *LLCL* filter (a) a series R_d inserted along the L_rC_r path (*LLCL*-1); (b) R_dC_f connected in parallel to only C_r (*LLCL*-2); and (c) R_dC_f connected in parallel to L_rC_r (*LLCL*-3). $V_i(t)$ and $V_g(t)$ denote the per phase VSC and the grid voltage, respectively.

respectively.

$$\left.\frac{i_g(s)}{V_i(s)}\right|_{V_g(s)=0} = \frac{Z_s(s)}{Z_s(s)Z_g(s) + Z_f(s)[Z_s(s) + Z_g(s)]} \tag{1}$$

$$\begin{cases} Z_f(s) = sL_f, Z_g(s) = sL_g \\ Z_s(s) = \left[R_d \left\| \frac{1}{sC_n} \right\| \left(L_r + \frac{1}{sC_r}\right)\right] + \frac{1}{sC_f} \end{cases} \tag{2}$$

It can be observed from Fig. 3 that this work uses a standard *LLCL* based *AC* filter as a fundamental building block for realizing the proposed *L-PT-L* filter. Therefore, in this section, we discuss a brief comparison of some of the popular passively damped *LLCL* filters and their limitations as motivation to utilize the proposed *L-PT-L* filtering scheme.

LLCL filters can be passively damped by adding a damping resistor, R_d, in various ways to the shunt L_rC_r branch [23], [24]. Such damping methods are typically preferred since the losses in R_d can be minimized without impacting the high-frequency impedance characteristics of converter side or grid side inductors [6], [25]. Fig. 4 elucidates some of the different methods popularly adopted in literature to dampen the *LLCL* filter resonance. The most straightforward way is to add a resistance in series with the L_rC_r branch as depicted in Fig. 4(a) (*LLCL*-1) [23]. This scheme reduces the effectiveness of the near-zero impedance offered by the L_rC_r branch at the switching frequency, f_{sw} and is generally not preferred. An alternative damping scheme is depicted in Fig. 4(b) (*LLCL*-2) [24]. Such a damping method uses an R_dC_f branch in parallel with the shunt capacitance (C_r) and achieves a -20 dB/dec roll-off characteristics for frequency, $f > f_{sw}$. Fig. 4(c) (*LLCL*-3) illustrates the popular passive damping method where the R_dC_f branch is added in parallel to the L_rC_r branch [24]. Such a configuration can provide a steeper -40 dB/dec high-frequency roll-off characteristics, which makes it favourable as compared to other passive damping schemes. Unfortunately, for such a configuration, both C_f and C_r have to be rated to handle the fundamental grid voltage amplitude (assuming $V_g(t) \approx V_c(t)$ due to negligible fundamental frequency voltage drop across L_g) which can easily, in turn, affect the voltage ratings of these capacitor components.

TABLE 1. Shunt Branch Impedance - *AC* Filter Configurations

Filter Type	Shunt Branch Impedance, $Z_s(s)$
$LLCL$-1	$sL_r + \frac{1}{sC_r} + R_d$
$LLCL$-2	$sL_r + \left[\frac{1}{sC_r} \| \left(R_d + \frac{1}{sC_f}\right)\right]$
$LLCL$-3	$\left(sL_r + \frac{1}{sC_r}\right) \| \left(R_d + \frac{1}{sC_f}\right)$
L-PT-L	$\left[R_d \| \frac{1}{sC_n} \| \left(sL_r + \frac{1}{sC_r}\right)\right] + \frac{1}{sC_f}$

TABLE 2. Shunt Branch Component Values - *AC* Filter Configurations

Filter Type	L_r (μH)	C_r (μF)	C_n (μF)	C_f (μF)	R_d (Ω)
$LLCL$-1	11.5	4.7	-	-	1
$LLCL$-2	11.5	4.7	-	11	10
$LLCL$-3	11.5	4.7	-	11	10
L-PT-L	15	4.7	1	15	5.5

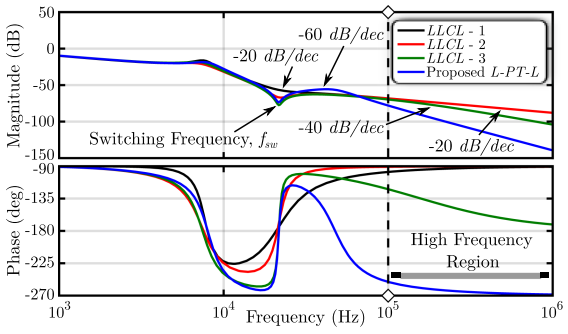

FIGURE 5. Frequency response plot ($i_g(s)/V_i(s)$) comparing the proposed *L-PT-L* filter with the conventionally damped *LLCL* filters.

The impedance of the shunt branch is denoted by $Z_s(s)$ and stated in Table 1 for the conventionally damped $LLCL$ filters as well as the L-PT-L filter.

Table 2 details the individual component parameters used for a comparative evaluation between the various *AC* filters. A comparison of $i_g(s)/V_i(s)$ between the passively damped $LLCL$ filters and the proposed L-PT-L filter is depicted in Fig. 5. The objective here is not to present any optimal filter designs but to showcase the superior high-frequency attenuation offered by the proposed L-PT-L filter from a qualitative perspective. The design considerations for the proposed L-PT-L filter will be discussed in detail in Section III.

From Fig. 5, it can be observed that the low-frequency characteristics of conventional damping $LLCL$ methods exhibit a similar phase response as the proposed L-PT-L filter. The conventionally damped $LLCL$ filters, as well as the proposed L-PT-L filter scheme, provide a similar attenuation at f_{sw} which would indicate a comparable reduction in the f_{sw} component of $i_g(t)$. The major difference can be observed in the high-frequency region where the L-PT-L filter not only has a higher attenuation across frequencies but also has a -60 dB/dec roll-off characteristics. A steeper high-frequency roll-off rate is always beneficial for the *AC* filter since it helps improve the attenuation offered to the differential mode (DM) EMI generated by the VSC [26], [27].

III. DESIGN CONSIDERATIONS FOR THE *L-PT-L* FILTER

In this section, the design considerations for the proposed L-PT-L filter have been elucidated in detail.

A. SELECTION OF INVERTER SIDE INDUCTOR, L_f

In a grid-tied VSC, the inverter side inductor (L_f) is typically selected to limit the worst-case current ripple (for e.g., $40-60\%$ of the fundamental frequency current component) as delineated in [5]. The peak-peak current ripple and L_f relationship, as well as its selection process, is discussed extensively in [17], [28]. An additional constraint on L_f selection is that f_{sw} current component should be restricted to a reasonable value since this can impact the current rating of L_r. The design considerations of L_f are similar to that of traditional $LLCL$ filters, and an interested reader is referred to [5], [10], [28] for additional details. The L_f was selected as 400 μH to keep the ripple current within 50% for this example.

B. DESIGN AND SELECTION OF SHUNT BRANCH ELEMENTS

The proposed L-PT-L filter utilizes five components in the shunt branch, namely three capacitors (C_n, C_r, C_f), an inductor (L_r), and a damping resistor (R_d). The shunt branch for the L-PT-L filter has a series L_rC_r path tuned at f_{sw} as in the case of a conventional $LLCL$ filter. In addition, C_n is added to provide a path for the high-frequency current ripple components ($f > f_{sw}$) and improve the high-frequency roll-off characteristics of the filter to -60 dB/dec. A damping resistor, R_d, is added in parallel to the L_rC_r and C_n to passively damp out any filter resonances. This parallel combination of L_rC_r, R_d, and C_n is finally connected in series with C_f.

1) EFFECT OF C_f ON L-PT-L FILTER

In the proposed L-PT-L filter, C_f should be selected such that $C_f >> C_r$ and $C_f >> C_n$. Further, the shunt capacitor, C_f, has to be selected to limit the fundamental frequency current component through the shunt branch of the L-PT-L filter. The total current, $i_c(s)$ that flows through C_f can be defined using (3).

$$i_c(s) = \frac{V_c(s)}{\left[R_d \left\| \frac{1}{sC_n} \right\| \left(L_r + \frac{1}{sC_r}\right)\right] + \frac{1}{sC_f}} \tag{3}$$

This can be simplified to reflect the current flowing through C_f at grid frequency, f_g. $V_c(t)$ can be approximated as $V_g(t)$ at f_g assuming negligible fundamental drop across L_g. Since the impedance of R_d is selected to be much lower than that of C_n and C_r at f_g, only the series combination of R_d and C_f determines the f_g component of current through the shunt

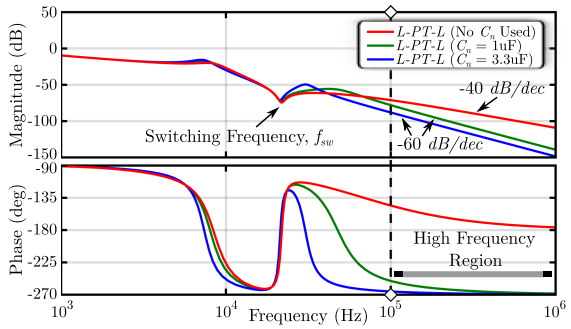

FIGURE 6. High-frequency roll-off characteristics of $i_g(s)/V_i(s)$ with and without C_n in the proposed *L-PT-L* filter network.

branch as shown in (4).

$$i_c(jw_g)\Big|_{w_g} = \left|\frac{V_g(jw_g)}{R_d + \dfrac{1}{jw_gC_f}}\right| \tag{4}$$

The impedance of R_d is chosen to be very small compared to that of C_f at f_g. Hence, C_f can be selected based on the power factor requirement of the system (for e.g 5% of reactive power at the rated load condition, P_{load}) and is described in (5).

$$C_f = 5\%\frac{P_{load}}{V_g(t)^2(2\pi f_g)} \tag{5}$$

For a power rating of 1.6 kW in this design, the C_f was selected as 15 μF.

2) EFFECT OF C_n ON *L-PT-L* FILTER

The capacitor, C_n, is used in the *L-PT-L* filter to achieve a -60 dB/dec roll-off characteristics in the high-frequency region, which can be advantageous to further suppress the current ripple at multiples of f_{sw} (including side-bands). A larger value of C_n would help improve the attenuation across frequencies in the high-frequency region. The only limiting factor is that C_n should be much smaller than C_f. The variation of C_n on the high-frequency roll-off characteristics of $i_g(s)/V_i(s)$ is illustrated in Fig. 6. It can be observed that although a -60 dB/dec attenuation can be achieved for all values of C_n, the roll-off characteristics itself start from different frequencies based on the specific values of C_n. A C_n value of 3.3 μF was used in the proposed filter.

3) EFFECT OF L_rC_r BRANCH ON *L-PT-L* FILTER

The selection of L_r and C_r is determined such that the resonant frequency, f_r, coincides with the operating switching frequency, f_{sw} of the power conversion system [5]. For the *L-PT-L* filter network, it is important that $C_r << C_f$ while selecting the value of C_r since this will lead to C_f having minimum impact on f_r of the L_rC_r branch.

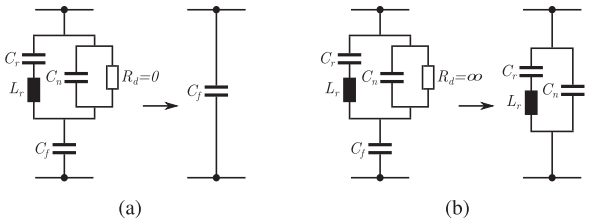

FIGURE 7. Effect of variation in R_d when (a) $R_d \to 0$; (b) $R_d \to \infty$. $C_f >> C_r$ and $C_f >> C_n$ for the proposed *L-PT-L* filter.

The resonant frequency, f_r, of the shunt branch can be approximated as

$$f_r \approx \frac{1}{2\pi \times \sqrt{L_r\dfrac{C_rC_f}{C_r + C_f}}} \tag{6}$$

Several combinations of L_r and C_r can lead to near zero impedance at the f_{sw}. Ideally, selecting a larger C_r increases the width of the series resonance notch at f_{sw}, leading to better performance in case of any drift in the component values (especially L_r) due to ageing, temperature variation, etc. Additionally, keeping the value of L_r small can aid in reducing the voltage rating of the inductor. For this design, L_r is chosen as 15 μH and C_r as 4.7 μF.

4) EFFECT OF DAMPING RESISTANCE, R_d ON *L-PT-L* FILTER

R_d plays an important role in the proposed *L-PT-L* filter since it not only aids in damping out the resonances but also reduces the voltage ratings of C_n and L_rC_r due to its specific placement. To elucidate the effect of using R_d on the shunt branch of the *L-PT-L* filter, two extreme conditions of R_d (0 and ∞) are evaluated as a first step. It can be easily delineated that when $R_d \to 0$, the shunt path can be modified as C_f and given in (7).

$$Z_s(s)\Big|_{R_d\to 0} = \frac{1}{sC_f} \tag{7}$$

It is interesting to note that when $R_d \to 0$, the *L-PT-L* filter decomposes into a *LCL* filter (as shown in Fig. 7(a)) with an un-damped resonant frequency, $w_r = \sqrt{\frac{L_f+L_g}{L_fL_gC_f}}$.

Alternatively when $R_d \to \infty$, $Z_s(s)$ is a function of only L_r, C_r and C_n (the effect of C_f can be ignored if it is sufficiently greater than C_r and C_n) as depicted in Fig. 7(b) and described in (8).

$$Z_s(s)\Big|_{R_d\to\infty} = \frac{(1 + sL_rC_r)}{sC_r + sC_n(1 + sL_rC_r)} \tag{8}$$

When no R_d is connected, the *L-PT-L* filter reduces to a *LCL-LC* filter [10]. There are two resonances associated with such a filter, and the resonant frequencies can be computed

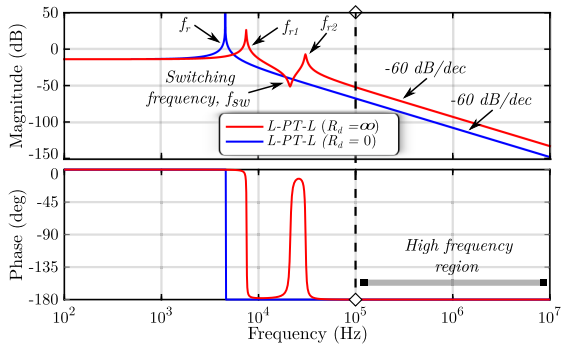

FIGURE 8. Effect of $R_d \to 0$ and $R_d \to \infty$ on $V_c(s)/V_i(s)$ for the proposed *L-PT-L* filter.

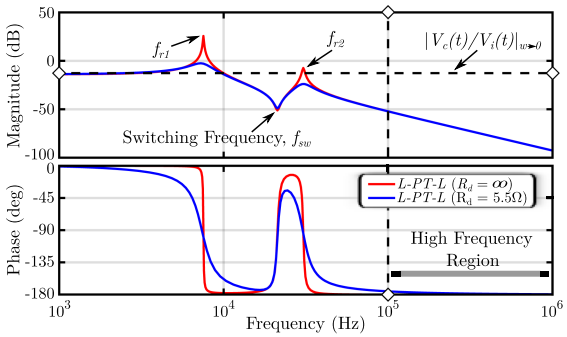

FIGURE 9. Selection of damping resistor, R_d for the proposed *L-PT-L* filter using the transfer function $V_c(t)/V_i(t)$ (based on a quality factor (*QF*) approach).

from (9) and (10).

$$\begin{cases} w_{r1} = \left(\dfrac{a_1 + a_2 - (a_3 + a_4 + a_5)^{1/2}}{a_6}\right)^{1/2} \\ w_{r2} = \left(\dfrac{a_1 + a_2 + (a_3 + a_4 + a_5)^{1/2}}{a_6}\right)^{1/2} \end{cases} \tag{9}$$

$$\begin{cases} a_1 = L_f L_g (C_r + C_n), \ a_2 = L_r C_r (L_f + L_g) \\ a_3 = L_f^2 L_2^2 (C_r + C_n)^2, \ a_4 = L_r^2 C_r^2 (L_f + L_g)^2 \\ a_5 = 2 L_f L_g L_r C_r (L_f + L_g)(C_r - C_n) \\ a_6 = 2 L_f L_g L_r C_r C_n \end{cases} \tag{10}$$

Fig. 8 illustrates both the extreme damping conditions $R_d \to 0$ and $R_d \to \infty$ by plotting $V_c(s)/V_i(s)$. A quality factor (QF) based approach as suggested in [19], [29] can be extended for the *L-PT-L* filter and used to determine a reasonable value of R_d.

The evaluation of QF is not straightforward in multi-resonant systems such as the proposed *L-PT-L* filter. To determine the QF of the filter, the transfer function relating the shunt-branch voltage to the inverter switching voltage, $V_c(t)/V_i(t)$ has to be determined as elucidated in (11).

$$\left.\frac{V_c(s)}{V_i(s)}\right|_{V_g(s)=0} = \frac{1}{1 + Z_f(s)\dfrac{Z_s(s) + Z_g(s)}{Z_s(s)}} \tag{11}$$

A frequency response plot for (11) is illustrated in Fig. 9 to showcase the impact of the damping resistance, R_d. Two

TABLE 3. Quality Factor With and Without R_d

R_d	$f_{r1} \approx 7.5\ kHz$	$f_{r2} \approx 30\ kHz$
$R_d \to \infty$	$QF \approx 90$	$QF \approx 2$
$R_d = 5.5\ \Omega$	$QF \approx 3.5$	$QF \approx 0.3$

resonances can be observed in the absence of R_d. The QF can now be evaluated at both the resonant frequencies, f_{r1} and f_{r2} as shown in (12).

$$QF\big|_{w_{r1}, w_{r2}} = \frac{|V_c(s)/V_i(s)|_{w=w_{r1}, w_{r2}}}{|V_c(s)/V_i(s)|_{w\to 0}} \tag{12}$$

It can be observed that the proposed placement of R_d can simultaneously damp out both these resonances. The R_d value for this design was selected as 5.5 Ω to obtain a low QF for this filter. The R_d and the corresponding QF values are tabulated in Table 3.

5) SHUNT BRANCH - VA RATINGS

The proposed *L-PT-L* filter can reduce the voltage ratings of the L_rC_r branch and C_n with the aid of the damping resistor, R_d which is connected in a parallel configuration. The voltage across R_d can be written as a function of $V_c(s)$ as described in (13).

$$V_{R_d}(s) = V_c(s) \frac{R_d \left\| \dfrac{1}{sC_n} \right\| \left(L_r + \dfrac{1}{sC_r}\right)}{R_d \left\| \dfrac{1}{sC_n} \right\| \left(L_r + \dfrac{1}{sC_r}\right) + \dfrac{1}{sC_f}} \tag{13}$$

The dominant voltage spectral component present in $V_c(t)$ is the fundamental frequency (f_g) voltage component [19] if the *AC* filter is designed appropriately to suppress the high-frequency harmonics in the grid current. The value of R_d is selected in such a manner that its impedance is much smaller as compared to the L_rC_r branch and C_n impedance at f_g. This fundamental voltage component in $V_c(t)$ gets split across R_d and C_f based on the impedances offered by them at f_g. Since the impedance of $C_f >> R_d$ (based on carefully selecting both C_f and R_d) at f_g, the voltage across R_d is only a fraction as compared to that across C_f as delineated in (14).

$$V_{R_d}(jw_g)\Big|_{w_g} = \left| V_c(jw_g) \frac{R_d}{R_d + \dfrac{1}{jw_g C_f}} \right| \tag{14}$$

As R_d is in parallel with C_n as well as the L_rC_r branch, f_g component of voltages across all these capacitor and resistor components (voltage drop across L_r can be neglected at f_g) would be similar.

This can be observed with the help of a frequency domain plot as illustrated in Fig. 10. The selected impedance of C_f at f_g is significantly (around 30 dB) greater than that of R_d leading to R_d (as well as C_r and C_n) needing to be rated for only a fraction of the per phase fundamental voltage ($V_g(t)$). The impedance difference between R_d and C_f at f_g is denoted as Z_{df} in Fig. 10.

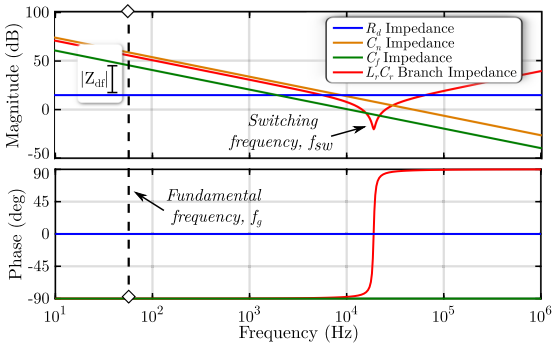

FIGURE 10. Impedance plot detailing the effect of R_d on the voltage ratings of C_n and C_r for the proposed *L-PT-L* filter.

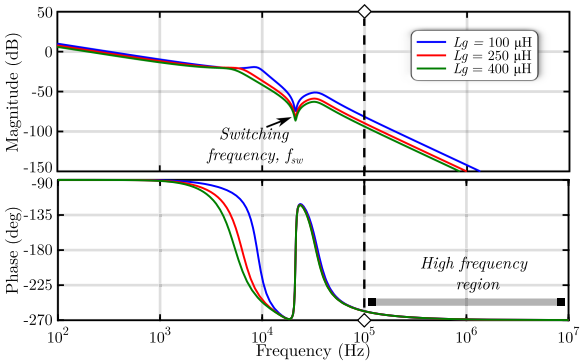

FIGURE 11. $i_g(s)/V_i(s)$ plot of *L-PT-L* filter to illustrate the impact of grid impedance variation.

Hence, the proposed passive damping scheme helps reduce the VA rating across C_r and C_n since their voltage rating gets clamped based on the fundamental voltage split between R_d and C_f.

C. SELECTION OF GRID SIDE INDUCTOR, L_g

The grid side inductor (L_g) can be selected based on the required attenuation at multiples of f_{sw} (and their side bands) since a near zero impedance is offered by the L_rC_r trap-based shunt branch at f_{sw} [5], [10]. Further, it is important to limit the fundamental frequency (f_g) voltage drop across $L_f + L_g$ to a reasonable value (for example, $5\%-10\%$ of the per phase voltage, $V_g(t)$) to restrict the amplitude of the DC link voltage. To determine the value of L_g, (15) and (16) can be utilized. The shunt branch can be approximated with C_n since its impedance will be much smaller as compared to R_d and L_rC_r branch when $f > f_{sw}$.

$$\left.\frac{i_g(jw)}{V_{DM}(jw)}\right|_{f>f_{sw}} = \frac{1/(L_f+L_g)}{(jw)\left[1+\dfrac{(jw)^2C_nL_fL_g}{(L_f+L_g)}\right]} \tag{15}$$

$$\left.L_g\right|_{f>f_{sw}} = \left|\frac{\dfrac{V_{dm}(jw)}{i_g(jw)} - jwL_f}{jw+(jw)^3L_fC_n}\right| \tag{16}$$

For this design, L_g was selected as 100 μH to obtain an attenuation of around -50 dB at around 40 kHz. The impact of grid inductance was not accounted during the design process as this corresponded to the worst case attenuation characteristics of the *L-PT-L* filter. To evaluate the impact of grid impedance variation, a sensitivity analysis was performed using different values of grid side inductors, and the results are plotted in Fig. 11. It can be observed that an increase in grid side inductance helps improve the attenuation characteristics of the proposed filter.

A flowchart is provided in Fig. 12 to summarize the electrical parameter selection for the proposed *L-PT-L* filter network.

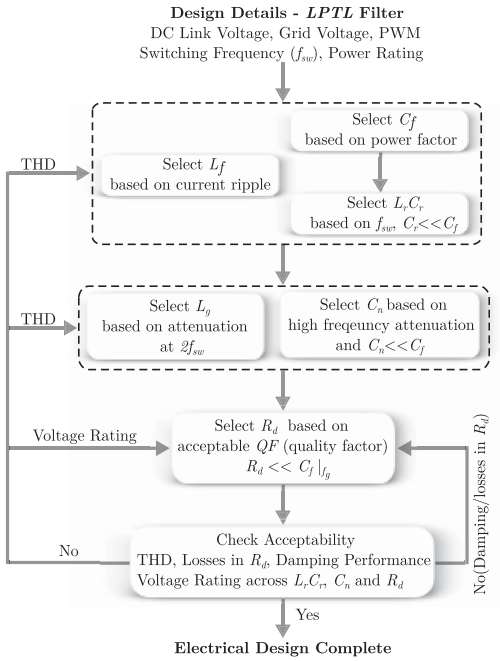

FIGURE 12. A flowchart depicting the design procedure for selecting the electrical components of the proposed *L-PT-L* filter network.

IV. COMPARATIVE EVALUATION OF FILTERING STRATEGIES

To understand the benefits of the proposed *L-PT-L* filter, two different scenarios are considered:

1) *Case 1:* Filter design for a low voltage (208 V, 60 Hz) grid-tied converter.
2) *Case 2:* Filter design for a medium voltage (4160 V, 60 Hz) grid-tied converter.

The size benefits of the proposed filtering approach will become apparent at higher voltages. The proposed *L-PT-L* filter is compared with other popular *LLCL* type *AC* filters in Fig. 4. Filter designs are carried out for the above two scenarios, and the design details are presented in Table 4 . To provide an equitable comparison between various filters (both low and medium voltage), an identical Q factor (for the

TABLE 4. Shunt Branch Component Values - *AC* Filter Configurations

Case 1: For Low Voltage Grid Interconnection					
Filter Type	L_r (μH)	C_r (μF)	C_n (μF)	C_f (μF)	R_d (Ω)
$LLCL$-2	11.5	4.7	-	11	10
$LLCL$-3	11.5	4.7	-	11	10
L-PT-L	15	4.7	0.1	11	5.5
$L_f = 400\ \mu H$ and $L_g = 100\ \mu H$ for all the above designs.					
Case 2: For Medium Voltage Grid Interconnection					
Filter Type	L_r (μH)	C_r (μF)	C_n (μF)	C_f (μF)	R_d (Ω)
$LLCL$-2	11.5	4.7	-	11	1
$LLCL$-3	11.5	4.7	-	11	1
L-PT-L	15	4.7	0.1	11	1
$L_f = 1000\ \mu H$ and $L_g = 10\ \mu H$ for all the above designs.					

TABLE 5. Performance Comparison of *AC* Filters

Case 1: For Low Voltage Grid Interconnection						
Filter Type	I_{Lr} (RMS)	V_{Cr} (RMS)	V_{Cn} (RMS)	V_{Cf} (RMS)	P_{Rd} (W)	I_{THD} (%)
$LLCL$-2	1.3 A	120 V	-	120 V	2.7 W	1.2%
$LLCL$-3	1.0 A	120 V	-	120 V	2.8 W	1.0%
L-PT-L	**1.0 A**	**3.1 V**	**3.4 V**	**120 V**	**2.1 W**	**1.2%**
Case 2: For Medium Voltage Grid Interconnection						
$LLCL$-2	15 A	2.4 kV	-	2.4 kV	110 W	1.5%
$LLCL$-3	7.8 A	2.4 kV	-	2.4 kV	137 W	0.7%
L-PT-L	**6.8 A**	**15 V**	**12 V**	**2.4 kV**	**146 W**	**1.1%**

admittance transfer function, $\frac{i_g(s)}{V_i(s)}$) has been selected for all the filters to obtain the filter component values.

A. PERFORMANCE COMPARISON OF AC FILTERS

Circuit simulations of the grid-tied inverter system with various filtering approaches (based on the designs in Table 4) are carried out for low voltage and medium voltage scenarios. The results are summarized in Table 5. The per-phase loss in the damping resistor (P_{Rd}) for the proposed filter is comparable to that in other state-of-the-art $LLCL$ type AC filter structures. It can be seen that the proposed L-PT-L filter offers excellent performance in terms of grid current total harmonic distortion (I_{THD}) while ensuring that the voltage ratings of the shunt branch capacitors, C_n, and C_r, are less than 5% of the grid voltage.

B. SIZE COMPARISON OF AC FILTERS

To understand the size benefits of fractionally rated components in the proposed L-PT-L filter, the filter designs in Table 4 are compared for low voltage and medium voltage scenarios. The VA ratings of the filter components are identified based on circuit simulations, and commercially off-the-shelf components are chosen for realizing the filter designs. For the MV filter designs, the higher voltage rated ($\approx$ 2.4 kV RMS) capacitors are realized by a series connection of four 1 kV rated capacitors. The details and the specific part numbers are presented in Table 6. It can be seen that the proposed L-PT-L filter only uses a single higher voltage-rated capacitor (C_f) as opposed to two higher voltage-rated capacitors (C_r, C_f) in $LLCL$-2 and $LLCL$-3 filters. Hence, the proposed L-PT-L filter offers a 19% reduction in the filter shunt branch volume for the low voltage scenario, and it offers a 36% reduction in the filter shunt branch volume for the medium voltage scenario as compared to other popular state-of-the-art $LLCL$ filters.

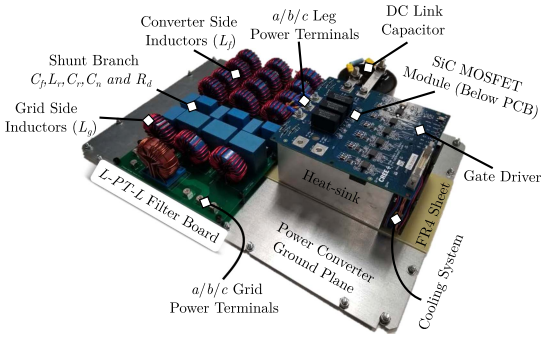

FIGURE 13. Realized hardware prototype of the grid-tied 3ϕ, 2-level VSC with the proposed *L-PT-L* filter network.

TABLE 6. Size Comparison of *AC* Filters

Case 1: For Low Voltage Grid Interconnection				
Filter Type	Component	VA rating	Vol (cm^3)	% Vol Reduction
$LLCL$-2	L_r (MSS7341-123MLD) C_r (MKS4F044706B00KB00) C_f (C4AF1BW5110F3FK)	3.4 125 62	42	-
$LLCL$-3	L_r (MSS7341-123MLD) C_r (MKS4F044706B00KB00) C_f (C4AF1BW5110F3FK)	2.5 125 64	42	-
L-PT-L	L_r (MSS6132-153MLC) C_r (16MU475MC14532) C_f (C4AF1BW5110F3FK) C_n (25MU104Z22012)	**2.9** **3.1** **140** **0.3**	**34**	**19%**
Case 2: For Medium Voltage Grid Interconnection				
Filter Type	Component	VA rating	Vol (cm^3)	% Vol Reduction
$LLCL$-2	L_r (XAL1010-103ME) C_r (4×C44PXGR5200RCSK) C_f (4×C44PXGR5470RASK)	205 12616 25420	8100	-
$LLCL$-3	L_r (XAL1010-103ME) C_r (4×C44PXGR5200RCSK) C_f (4×C44PXGR5470RASK)	96 18990 27900	8100	-
L-PT-L	L_r (XAL1010-153MED) C_r (16MU475MC14532) C_f (4×C44PXGR5470RASK) C_n (25MU104Z22012)	**105** **98** **34412** **2.5**	**5620**	**36%**

C. COST COMPARISON OF AC FILTERS

A few simplifying assumptions are adopted to compare the cost of the various filtering solutions. The cost difference is attributed mostly to C_r (impact of C_n used for the L-PT-L filter is very minimal). Two fractionally rated capacitors are used in the proposed approach as opposed to the full-rated capacitor in $LLCL$-2 and $LLCL$-3 options. The cost model based on [30] and [31] is adopted in this work, where the cost (in US dollars) of the film capacitor is linearly proportional to

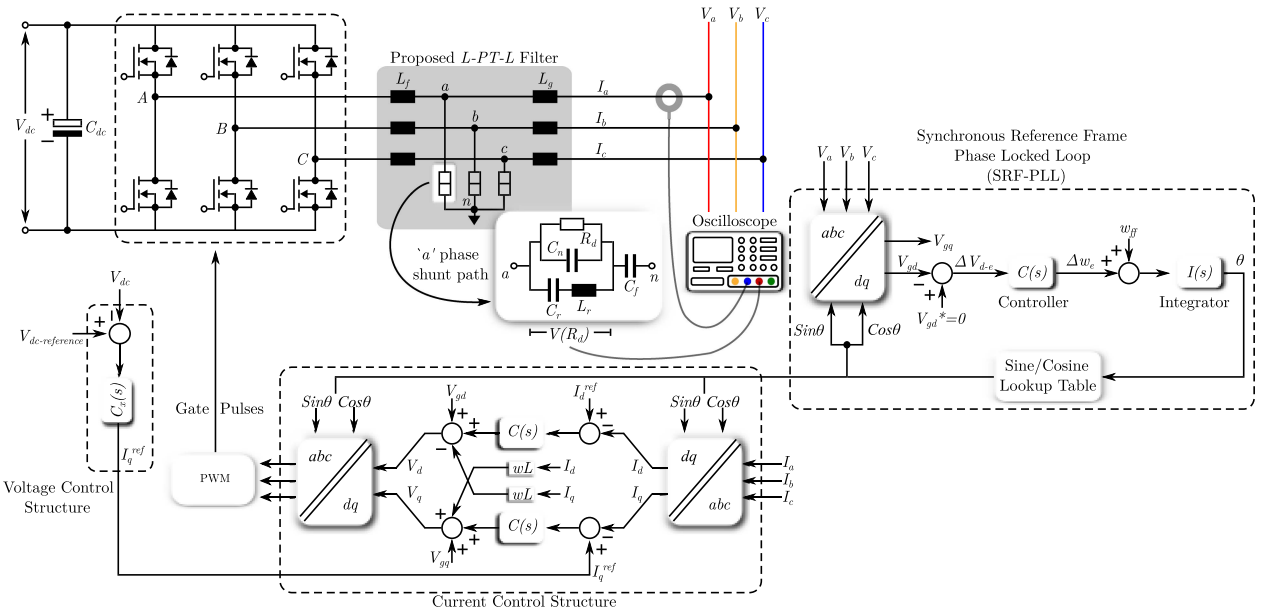

FIGURE 14. 3ϕ, 2-level grid-tied VSC with conventional feedback control system for the proposed *L-PT-L* filter network.

the rated capacitance, C_r in μF and the voltage, V_{Cr}, in V.

$$\Sigma_{FILM} = a_F + b_F.V_{Cr} + c_F.C_r \tag{17}$$

where $a_F = 17.64$, $b_F = 0.0391$, $c_F = 0.2014$. It must be noted that the cost comparison presented assumes that a single capacitor is sufficient to meet both the required capacitance and the RMS current rating of the capacitor. As the root mean square error of the model itself is around 11.7 USD, the comparison is only presented for the medium voltage grid interconnection scenario. For *LLCL*-2 and *LLCL*-3 filters, the cost of capacitor C_r for all three phases is computed to be 525 USD (the actual capacitors selected have a pricing of around 550 USD). For the proposed *L-PT-L* filter, the model estimates the cost as 60 USD. The error in the model tends to be higher for low voltage rated capacitors, and the overall cost of C_r and C_n for the *L-PT-L* filter is only 12 USD.

V. RESULTS AND DISCUSSION

The proposed *L-PT-L* filter was designed and developed in the laboratory and integrated with a 2-level, 3ϕ VSC as depicted in Fig. 13. Fig. 14 illustrates the measurement details and the conventional feedback control methodology adopted for the 2-level, 3ϕ VSC. The grid-tied VSC was operated in the rectifier mode with a resistive load of 100 Ω connected to the DC link. The per-phase voltage of the utility grid was 120 V (RMS), and the DC link of the VSC was maintained at 400 V. The switching frequency of the VSC was selected as 22 kHz. The power converter's output was 1.6 kW and the converter efficiency was greater than 96%. The parameters of the implemented *L-PT-L* filter are given in Table 7.

The feedback control system included a DC link voltage regulator and grid current compensators. Grid current control was implemented using PI regulators in the dq frame. The unit vectors for the frame transformations ($abc \leftrightarrow dq$) were derived by implementing a synchronous-reference-frame-based phase-locked loop (SRF-PLL). The feedback control system was implemented on a digital platform (TMS320F28335). The sampling frequency for the digital control implementation was selected to be the same as the switching frequency (22 kHz) of the grid-tied VSC.

Several experiments were conducted using the grid-tied VSC to evaluate the performance of the proposed *L-PT-L* filter. Performance metrics such as (a) the THD in the grid currents, (b) the voltage ratings across R_d, C_n, and L_rC_r branches,

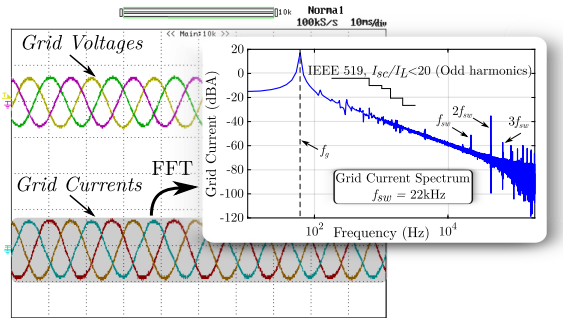

FIGURE 15. Phase voltages [200 V/div] and grid currents [10 A/div] versus time [10 ms/div] during the steady state operation of the grid-tied VSC with the proposed *L-PT-L* filter. The experimentally measured FFT of the grid current has been illustrated as well.

TABLE 7. Implemented *L-PT-L* Filter Parameters

L_f (μH)	L_g (μH)	L_r (μH)	C_r (μF)	C_n (μF)	C_f (μF)	R_d (Ω)
400	100	15	4.7	3.3	15	5.5

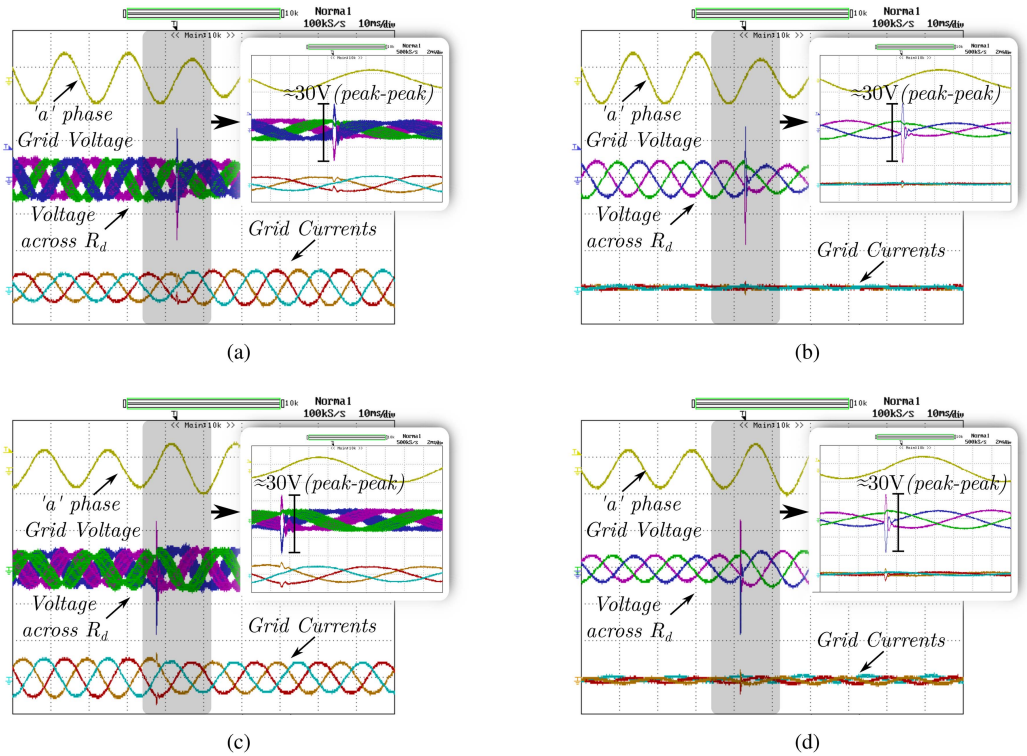

FIGURE 16. Experimental results showcasing the grid currents and voltages across R_d during a grid voltage disturbance. (a) and (b) showcase a per-phase grid voltage sag from 120 V (RMS) to 90 V (RMS), while (c) and (d) depict a per-phase grid voltage swell from 90 V (RMS) to 120 V (RMS). The converter is in the OFF state in (b) and (d). The plot scales are - grid voltage [200 V/div], voltage across R_d [10 V/div], and time [10 ms/div]. The grid current scale is [20 A/div] in (a), (b), and (c) while it is [10 A/div] in (d).

and (c) the effectiveness of the proposed damping scheme during step grid voltage disturbances were evaluated using experiments conducted on the laboratory prototype.

A. HARMONIC DISTORTION - GRID CURRENTS

The effectiveness of the proposed *L-PT-L* filter to achieve the desired filtering was validated experimentally by observing the frequency spectrum of the grid-side current under steady-state conditions. The experimentally measured frequency spectrum of the grid-current is presented in Fig. 15 (in dBA versus frequency). The permissible harmonic limits on the current injected into the grid by a power converter as per IEEE 519-2014 are superimposed on top of the grid-current frequency spectrum in Fig. 15. These harmonic limits are specified for a worst-case weak-grid condition ($I_{sc}/I_L < 20$).

It can be observed that the individual harmonic components in the grid currents are well within the harmonic limits as stipulated by IEEE 519-2014. Further, the THD of the grid-current was measured to be around 1%. The effectiveness of the *LC* trap is evident from the improved attenuation offered to the switching frequency (22 kHz) spectral component. As delineated from Fig. 15, the proposed filter can meet the required harmonic distortion limits.

B. PASSIVE DAMPING - GRID SIDE VOLTAGE DISTURBANCES

The effectiveness of the proposed passive damping scheme is validated by creating step disturbances in the grid voltages. The disturbances were created under normal operating conditions of the VSC and when the VSC was switched OFF. In case the VSC is switched OFF while the *AC* filter is still connected to the grid, any grid side voltage disturbances can trigger unwanted filter resonances unless the resonance is suppressed by means of passive damping [19].

In Figs. 16(a) and (b), a 25% symmetrical voltage sag is created while in Figs. 16(c) and (d), a symmetrical voltage swell of 25% is created. It can be observed that such grid-side voltage disturbances do not trigger any unwanted *LC* resonances, which in turn demonstrates the effectiveness of the proposed passive damping scheme for the *L-PT-L* filter. The overall loss in damping resistors under normal operating conditions of the VSC was measured to be ≈ 9 W.

It is to be noted that the *L-PT-L* filter resonances (refer Fig. 8) lie above the bandwidth of the grid current control loop (≈ 1 kHz) in our design and hence, the resonances cannot be mitigated by means of the control system using active damping. Further, active damping schemes impose an additional constraint that the power conversion system must always be operational.

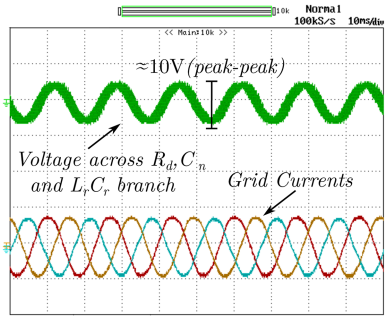

FIGURE 17. Experimental results showcasing voltage across the shunt branch (Scale: Voltage [10 V/div], current [10 A/div], and time [10 ms/div]).

TABLE 8. Individual Harmonic Voltages Across R_d, C_n, and L_rC_r branch Experimental Results - f_{sw} = 22 Khz

f_g = 60 Hz	f_{sw} = 22 kHz	$2f_{sw}$ = 44 kHz	$3f_{sw}$ = 66 kHz
3.22 V	0.190 V	0.709V	0.158 V

C. FRACTIONAL VOLTAGE RATING - SHUNT COMPONENTS

One of the advantages of the proposed *L-PT-L* filter was the reduced voltage ratings of the components in the shunt branch (R_d, C_n and L_rC_r). To validate this claim, the voltage across the damping resistor (in one of the phases) is measured and shown in Fig. 17. The peak-to-peak voltage across C_n, R_d, and L_rC_r is measured to be around 10 V. This is achieved by appropriately selecting R_d, as explained in Section III. The individual fundamental and harmonic voltages across R_d have been provided in Table 8. Hence, it has been demonstrated that some of the shunt components of the proposed *L-PT-L* filter can have a fractional voltage rating leading to a reduced overall VA rating.

VI. CONCLUSION

In this work, an *AC* filter for a grid-tied voltage source converter (VSC) was proposed and analyzed to suppress the unwanted current harmonics in the grid currents. It was delineated that the proposed passively damped *L-PT-L* filter can achieve a −60 dB/dec high-frequency roll-off characteristics. It was also demonstrated that two of the shunt-connected capacitors could be rated for a fraction of the fundamental voltage due to the specific placement of the damping resistor in the proposed filter configuration. This results in two of the shunt-connected capacitors to have smaller voltage ratings. A detailed analysis of the working, design, and effectiveness of the *L-PT-L* filter was elucidated in this article. To compare the performance of state-of-the-art *LLCL* filters with the proposed *L-PT-L* filter in an equitable manner, a Q-factor based design methodology was used to select the parameter values for all the filters. It is delineated that the proposed approach can offer 19% and 36% filter shunt branch volume reduction for low voltage (208 V, 60 Hz) and medium voltage (4.16 kV, 60 Hz) grid-tie inverter systems, respectively, compared to state-of-the-art *LLCL* filters. A hardware prototype of a 208 V, 60 Hz 3ϕ, grid-tied VSC along with the proposed *L-PT-L* filter was developed in the laboratory, and its performance was experimentally validated.

REFERENCES

[1] Z. Chen, J. M. Guerrero, and F. Blaabjerg, "A review of the state of the art of power electronics for wind turbines," *IEEE Trans. Power Electron.*, vol. 24, no. 8, pp. 1859–1875, Aug. 2009, doi: 10.1109/TPEL.2009.2017082.

[2] "IEEE recommended practice and requirements for harmonic control in electric power systems," IEEE Standard 519-2014 (Revision of IEEE Standard 519-1992), Jun. 2014, doi: 10.1109/IEEESTD.2014.6826459.

[3] M. Liserre, F. Blaabjerg, and S. Hansen, "Design and control of an LCL-filter-based three-phase active rectifier," *IEEE Trans. Ind. Appl.*, vol. 41, no. 5, pp. 1281–1291, Sep./Oct. 2005.

[4] K. Jalili and S. Bernet, "Design of *LCL* filters of active-front-end two-level voltage-source converters," *IEEE Trans. Ind. Electron.*, vol. 56, no. 5, pp. 1674–1689, May 2009.

[5] W. Wu, Y. He, and F. Blaabjerg, "An LLCL power filter for single-phase grid-tied inverter," *IEEE Trans. Power Electron.*, vol. 27, no. 2, pp. 782–789, Feb. 2012, doi: 10.1109/TPEL.2011.2161337.

[6] J. Fang, X. Li, X. Yang, and Y. Tang, "An integrated Trap-LCL filter with reduced current harmonics for grid-connected converters under weak grid conditions," *IEEE Trans. Power Electron.*, vol. 32, no. 11, pp. 8446–8457, Nov. 2017.

[7] Y. Sozer, D. A. Torrey, and S. Reva, "New inverter output filter topology for PWM motor drives," *IEEE Trans. Power Electron.*, vol. 15, no. 6, pp. 1007–1017, Nov. 2000.

[8] M. Sanatkar-Chayjani and M. Monfared, "High-order filter design for high-power voltage-source converters," *IEEE Trans. Ind. Electron.*, vol. 65, no. 1, pp. 49–58, Jan. 2018.

[9] W. Wu, Y. Sun, Z. Lin, T. Tang, F. Blaabjerg, and H. S. Chung, "A new *LCL*-Filter with in-series parallel resonant circuit for single-phase grid-tied inverter," *IEEE Trans. Ind. Electron.*, vol. 61, no. 9, pp. 4640–4644, Sep. 2014.

[10] F. Li, X. Zhang, H. Zhu, H. Li, and C. Yu, "An LCL-LC filter for grid-connected converter: Topology, parameter, and analysis," *IEEE Trans. Power Electron.*, vol. 30, no. 9, pp. 5067–5077, Sep. 2015.

[11] W. Wu, Y. Zhang, F. Blaabjerg, and H. S.-H. Chung, "A new type of three-phase asymmetric-LCL power filter for grid-tied voltage source inverter with step-up transformer," *IEEE Trans. Ind. Electron.*, vol. 69, no. 12, pp. 11936–11945, Dec. 2022, doi: 10.1109/TIE.2021.3131867.

[12] X. Li, P. Lin, and Y. Tang, "Magnetic integration of LTL filter with two *LC*-Traps for grid-connected power converters," *IEEE Trans. Emerg. Sel. Topics Power Electron.*, vol. 6, no. 3, pp. 1434–1446, Sep. 2018, doi: 10.1109/JESTPE.2017.2764060.

[13] K. Koiwa, H. Takahashi, T. Zanma, K.-Z. Liu, K. Natori, and Y. Sato, "A novel filter with high harmonics attenuation and small dimension for grid-connected inverter," *IEEE Trans. Power Electron.*, vol. 38, no. 2, pp. 2202–2214, Feb. 2023, doi: 10.1109/TPEL.2022.3207432.

[14] S. Gulur, V. M. Iyer, and S. Bhattacharya, "A CM filter configuration for grid-tied voltage source converters," *IEEE Trans. Ind. Electron.*, vol. 67, no. 10, pp. 8100–8111, Oct. 2020, doi: 10.1109/TIE.2019.2949530.

[15] R. N. Beres, X. Wang, F. Blaabjerg, M. Liserre, and C. L. Bak, "Optimal design of high-order passive-damped filters for grid-connected applications," *IEEE Trans. Power Electron.*, vol. 31, no. 3, pp. 2083–2098, Mar. 2016, doi: 10.1109/TPEL.2015.2441299.

[16] J. Xu, J. Yang, J. Ye, Z. Zhang, and A. Shen, "An LTCL filter for three-phase grid-connected converters," *IEEE Trans. Power Electron.*, vol. 29, no. 8, pp. 4322–4338, Aug. 2014, doi: 10.1109/TPEL.2013.2292000.

[17] R. N. Beres, X. Wang, M. Liserre, F. Blaabjerg, and C. L. Bak, "A review of passive power filters for three-phase grid-connected voltage-source converters," *IEEE Trans. Emerg. Sel. Topics Power Electron.*, vol. 4, no. 1, pp. 54–69, Mar. 2016.

[18] R. Pena-Alzola, M. Liserre, F. Blaabjerg, R. Sebastian, J. Dannehl, and F. W. Fuchs, "Analysis of the passive damping losses in LCL-Filter-Based grid converters," *IEEE Trans. Power Electron.*, vol. 28, no. 6, pp. 2642–2646, Jun. 2013.
[19] P. Channegowda and V. John, "Filter optimization for grid interactive voltage source inverters," *IEEE Trans. Ind. Electron.*, vol. 57, no. 12, pp. 4106–4114, Dec. 2010.
[20] M. Saleem, K.-Y. Choi, and R.-Y. Kim, "Resonance damping for an LCL filter type grid-connected inverter with active disturbance rejection control under grid impedance uncertainty," *Int. J. Elect. Power Energy Syst.*, vol. 109, pp. 444–454, 2019, doi: 10.1016/j.ijepes.2019.02.004.
[21] G. Ma, C. Xie, C. Li, J. Zou, and J. M. Guerrero, "Passivity-based design of passive damping for LCL-Type grid-connected inverters to achieve full-frequency passive output admittance," *IEEE Trans. Power Electron.*, vol. 38, no. 12, pp. 16048–16060, Dec. 2023, doi: 10.1109/TPEL.2023.3313106.
[22] J. Fang, X. Li, and Y. Tang, "A review of passive power filters for voltage-source converters," in *Proc. Asian Conf. Energy, Power Transp. Electrific.*, 2016, pp. 1–6, doi: 10.1109/ACEPT.2016.7811547.
[23] W. Wu et al., "A robust passive damping method for LLCL-filter-based grid-tied inverters to minimize the effect of grid harmonic voltages," *IEEE Trans. Power Electron.*, vol. 29, no. 7, pp. 3279–3289, Jul. 2014, doi: 10.1109/TPEL.2013.2279191.
[24] W. Wu, Y. He, T. Tang, and F. Blaabjerg, "A new design method for the passive damped LCL and LLCL filter-based single-phase grid-tied inverter," *IEEE Trans. Ind. Electron.*, vol. 60, no. 10, pp. 4339–4350, Oct. 2013, doi: 10.1109/TIE.2012.2217725.
[25] M. Huang, F. Blaabjerg, and P. C. Loh, "The overview of damping methods for three-phase grid-tied inverter with LLCL-filter," in *Proc. 16th Eur. Conf. Power Electron. Appl.*, 2014, pp. 1–9, doi: 10.1109/EPE.2014.6911055.
[26] S. Gulur, V. M. Iyer, and S. Bhattacharya, "A CM filter configuration for grid-tied voltage source converters," *IEEE Trans. Ind. Electron.*, vol. 67, no. 10, pp. 8100-8111, Oct. 2020, doi: 10.1109/TIE.2019.2949530.
[27] M. Hartmann, H. Ertl, and J. W. Kolar, "EMI filter design for a 1 MHz, 10 kW three-phase/level PWM rectifier," *IEEE Trans. Power Electron.*, vol. 26, no. 4, pp. 1192–1204, Apr. 2011, doi: 10.1109/TPEL.2010.2070520.
[28] A. A. Rockhill, M. Liserre, R. Teodorescu, and P. Rodriguez, "Grid-filter design for a multimegawatt medium-voltage voltage-source inverter," *IEEE Trans. Ind. Electron.*, vol. 58, no. 4, pp. 1205–1217, Apr. 2011, doi: 10.1109/TIE.2010.2087293,.
[29] A. K. Balasubramanian and V. John, "Analysis and design of split-capacitor resistiveinductive passive damping for LCL filters in grid-connected inverters," *IET Power Electron.*, vol. 6, no. 9, pp. 1822–1832, Nov. 2013, doi: 10.1049/iet-pel.2012.0679.
[30] R. Burkart and J. W. Kolar, "Component cost models for multi-objective optimizations of switched-mode power converters," in *Proc. IEEE Energy Convers. Congr. Expo.*, 2013, pp. 2139–2146, doi: 10.1109/ECCE.2013.6646971.
[31] Y. Prabowo, S. Sharma, S. Bhattacharya, A. K. Tripathi, and V. Bhavaraju, "ZVS boundary analysis and design guideline of MV grid-compliant solid-state transformer for DC fast charger applications," *IEEE Trans. Transport. Electrific.*, vol. 9, no. 4, pp. 4964–4980, Dec. 2023, doi: 10.1109/TTE.2022.3229223.

SRINIVAS GULUR (Member, IEEE) received the B.E. degree in electrical and electronics engineering from Anna University, Chennai, India, in 2010, the M.S. degree in electrical engineering systems from the University of Michigan, Ann Arbor, MI, USA in 2013, and the Ph.D. degree in electrical engineering from NC State University, Raleigh, NC, USA, in 2020.

In 2020, he was a Postdoctoral Researcher with NC State University. He was a Senior Power Electronics Engineer with Lucid USA Inc. from 2020 to 2023 and as a Staff EMC Engineer with Archer Aviation Inc. from 2023 to 2024. He is currently the EMC Manager with Archer Aviation Inc. His research interests include EMI / EMC modeling and mitigation schemes for power electronic converters (conducted and radiated emissions / susceptibility), differential mode (DM), and common mode (CM) filter designs, and feedback control strategies for power conversion systems.

VISHNU MAHADEVA IYER (Senior Member, IEEE) received the B.Tech. degree in electrical and electronics engineering from the College of Engineering, Trivandrum, India, in 2011, the M.E. degree in electrical engineering from the Indian Institute of Science (IISc), Bengaluru, India, in 2013, and the Ph.D. degree in electrical engineering from NC State University, Raleigh, NC, USA, in 2020.

He worked as a Lead Engineer with GE Research, Niskayuna, NY, USA, in 2020 and as a Power Electronics Engineer with GE Research, Bengaluru, India, from 2013 to 2015. In September 2020, he joined as an Assistant Professor with the Department of Electrical Engineering, IISc Bengaluru. His research interests include resonant and soft-switched power converters, high-frequency magnetics, control and stability of power electronic converters, and partial power processing.

SUBHASHISH BHATTACHARYA (Fellow, IEEE) received the B.E. degree in electrical engineering from the Indian Institute of Technology - Roorkee, Roorkee, India, the M.E. degree in electrical engineering from the Indian Institute of Science, Bengaluru, India, and the Ph.D. degree in electrical engineering from the University of Wisconsin-Madison, Madison, WI, USA, in 2003. He was with the FACTS and Power Quality Division, Westinghouse/Siemens Power T&D, during 1998–2005. In 2005, he joined NC State University, Raleigh, NC, USA, where he is currently the Duke Energy Distinguished Professor in electrical and computer engineering. He is currently a founding Faculty Member of NSF FREEDM Systems Center and DOE Power America Institute.

A part of his Ph.D. research on active power filters was commercialized by York Corporation for air-conditioner chillers. His research interests include solid-state transformers, MV power converters, FACTS, utility applications, high-frequency magnetics, and power conversion applications of SiC devices.